Supporting Information

Soluble Gd_6Cu_{24} Clusters: Effective Molecular Electrocatalysts for Water Oxidation

Jia-Nan Chen,† Zhong-Hua Pan,† Qi-Hao Qiu, Cheng Wang, La-Sheng Long, Lan-Sun Zheng, and Xiang-Jian Kong*

Collaborative Innovation Center of Chemistry for Energy Materials, State Key Laboratory of Physical Chemistry of Solid Surface and Department of Chemistry, College of Chemistry and Chemical Engineering, Xiamen University, Xiamen 361005, China

*E-mail: xjkong@xmu.edu.cn

1. Experimental Section:

1.1 Chemicals: $Gd(ClO_4)_3$ (1.0 mol·L^{-1}), Copper(II) Perchlorate Hexahydrate ($Cu(ClO_4)_2·6H_2O$), Imidazole ($C_3H_4N_2$), Sodium acetate ($NaAc·3H_2O$), L-Alanine ($C_3H_7NO_2$) and Sodium hydroxide (NaOH) are analytical grade, and used as received without further purification.

1.2 Sample Preparation.

1.2.1 Preparation of aqueous solutions of $Gd(ClO_4)_3$ (1.0 mol·L^{-1}).

Gadolinium oxide (0.125 mol, 45.313 g) was dissolved by slowly adding perchloric acid aqueous solution (70.0% -72.0%, 64.0mL) at about 80 °C. Aqueous solution of $Gd(ClO_4)_3$ (1.0 mol L^{-1}) was obtained by diluting theconcentrated solution to 250.00 mL with deionized water.

1.2.2 Synthesis of $[Gd_6Cu_{24}(IM)_{12}(L\text{-}Al)_{12}(\mu_3\text{-}OH)_{30}(\mu_2\text{-}OH)_6(CO_3)(H_2O)_{24}]·(ClO_4)_{16}·(H_2O)_6$ (Gd_6Cu_{24}-IM)

$Gd(ClO_4)_3$ (1.0 mol L^{-1}, 1.5 mL), $Cu(ClO_4)_2·6H_2O$ (0.5 mol L^{-1}, 6 mL) and L-Alanine (3.0 mol) were put into a 50 mL round bottom flask at the same time， 1.0 mol/L NaOH aqueous solution was added

dropwise in the above mixture until to adjust the pH (pH ≈ 6.2~6.8), and the solution turned from light blue to dark blue. After the mixture was heated to reflux for two hours at 120 °C, 3 mmol of imidazole solid was added, stirring was continued for 2 h, and then filtered into a beaker while hot. Bule bulk crystals of **Gd_6Cu_{24}-IM** were obtained in **31%** yield (based on $Gd(ClO_4)_3$) after the filtrate was kept at room temperature for at least 1 month. For $C_{73}H_{216}Cu_{24}Gd_6N_{36}O_{157}Cl_{16}$ (FW = 7146.49): C, 12.27; H, 3.05; N, 7.06. Found: C, 12.28; H, 3.02; N, 7.15. IR (KBr, cm^{-1}): 3412 (s), 3237 (s), 3124 (s), 2965 (w), 2868 (w), 2014 (w), 1621 (s), 1394 (s), 1100 (s), 934 (m), 851 (w), 752 (m), 632 (s).

1.2.2 Synthesis of $[Gd_6Cu_{24}(Ac)_6(L\text{-}Al)_{12}(\mu_3\text{-}OH)_{30}(\mu_2\text{-}OH)_6Cl(H_2O)_{24}]\cdot(ClO_4)_{11}\cdot(H_2O)_{19}$ (Gd_6Cu_{24}-AC)

Gd_6Cu_{24}-AC was synthesized by the same method of **Gd_6Cu_{24}-IM** except the substitution of imidazole to $NaAc{\cdot}3H_2O$. $C_{48}H_{206}Cu_{24}Gd_6N_{12}O_{159}Cl_{12}$ (FW = 6390.21, based on 20 coordinated water): C, 9.01; H, 3.34; N, 2.63. Found: C, 9.11; H, 3.41; N, 2.58. IR (KBr, cm^{-1}): 3412 (s), 3147 (w), 2965 (w), 2868 (w), 2014 (w), 1621 (s), 1394 (s), 1100 (s), 934 (m), 851 (w), 752 (m), 632 (s).

2. Characterization.

2.1 Measurements. An infrared spectrum was recorded on a Nicolet AVATAR FT-IR360 spectrophotometer with pressed KBr pellets. Microanalyses of C, H and N were carried out with a CE instruments EA 1110 elemental nanlyzer. Thermogravimetric analysis (TGA) curve was prepared on a SDT-Q600 thermal analyzer. The powder X-ray diffraction (XRD) patterns were recorded on Rigaku Ultima IV diffractionmeter using Cu Kα radiation at 25 kV and 100 mA. UV−visible spectra were recorded using a Cary 5000 UV-Vis spectrometer (Viarian, USA).

2.2 Single Crystal X-ray Diffraction Determination of single crystals of Gd_6Cu_{24}. Data of the clusters Data of **Gd_6Cu_{24}** were collected on a Rigaku SuperNova X-Ray single crystal diffractometer SmartLab-SE using graphite monochromatized MoKα radiation (λ = 0.71073 Å) at 100 K. Absorption corrections were applied using the multiscan program SADABS.[1] The structures were solved by direct methods (SHELXTL Version 5.10),[2] and the non-hydrogen atoms were refined anisotropically by full-matrix least-squares method on F^2. The hydrogen atoms of organic ligand were generated geometrically (C-H = 0.96 Å, N-H = 0.90 Å). Crystal data, as well as details of the data collection and

refinement, for the complexes are summarized in Table S1. CCDC number of 2244617-2244618 for clusters contains the supplementary crystallographic data for this paper.

3. Electrochemical methods

The electrochemical measurements were performed in the cell equipped with three electrodes, working electrode, counter electrode (Pt wire) and reference electrode (Ag/AgCl, saturated KCl, +0.20 V vs. NHE). Electrochemical studies, cyclic Voltammetry (CV), linear scan voltammetry (LSV), differential pluse voltammetry (DPV) and controlled-potential electrolysis (CPE) experiments, were conducted at room temperature using Electrochemical workstation (CHI 760E, Shanghai Chenhua). For CV, DPV measurement, the 0.07 cm^2 glassy carbon (GC) electrodes were as the working electrode. Working electrode pretreatment before each measurement included polishing with 0.05 μm alumina paste followed by rinsing with water, and drying in air. CVs were collected at 100mV/s unless otherwise mentioned. No IR compensation was employed. For CPE measurements, the clean and dry Indium tin oxide (ITO) glasses served as the working electrodes. All redox potentials in the present work are reported versus NHE by adding 0.2V to the measured potential. In typical experiments, a stream of N_2 in atmospheric pressure was bubbled into the solution for 20 min prior to scanning. The generated O_2 in the headspace was quantified by gas chromatography with a thermal conductive detector with argon as carrier gas (AuLight GC 7920). Faradic efficiency (FE (%)) was calculated based on following equation:

$$FE(\%) = \frac{4 * amount\ of\ O_2\ (moles) * 100}{n\ (moles\ of\ electrons)}$$

Where $n = \frac{Q}{F}$

4. TOF calculation

TOF is the abbreviation of Turnover frequency, representing the number of reactions that occur per unit time and unit active site under a given temperature, pressure, reactant ratio and a certain degree of reaction. In Equation (1), the diffusive current i_d was estimated using this couple ($\alpha = 0.5$, $n_d = 2$), A is the area of the electrode, D is the diffusion coefficient, R is ideal gas constant, T is temperature, F is Faraday constant. The measured maximum catalytic current i_c varied linearly with the concentration of catalysts, consistent with Equation (2). In Equation (2), k_{cat} is the catalytic rate

constants, referred as turnover frequency (TOF) of the catalyst, $n_c = 4$ is the number of electrons transferred to generate 1 mol O_2. k_{cat} of the catalyst was calculated on the basis of Equation (3).

$$i_d = 0.496 n_d F A [CAT] (\alpha n_d F \nu D/RT)^{1/2} \quad (1)$$

$$i_c = n_c F A [CAT] (D k_{cat})^{1/2} \quad (2)$$

$$i_c/i_d = 0.323\ n_c/\alpha^{1/2} n_d^{3/2} (k_{cat}/\nu)^{1/2} \quad (3)$$

Table S1 Single Crystal X-ray Structure Refinement of **Gd_6Cu_{24}-IM** and **Gd_6Cu_{24}-AC**.

Complex	**Gd_6Cu_{24}-IM**	**Gd_6Cu_{24}-AC**
Formula	$C_{73}H_{216}Cu_{24}Gd_6N_{36}O_{157}Cl_{16}$	$C_{48}H_{206}Cu_{24}Gd_6N_{12}O_{159}Cl_{12}$
Mr	7146.49	6390.21
T(K)	100.01(10)	100.01(10)
cryst syst	trigonal	triclinic
space group	*R-3*	*P-1*
A, Å	20.0889(6)	18.7431(5)
B, Å	20.0889(6)	18.7639(5)
C, Å	57.4977(9)	19.9485(6)
V, Å^3	20095.2(12)	5524.1(3)
Z,	3	1
Dc, (g cm^{-3})	1.733	1.788
μ, (mm^{-1})	13.733	1698
θ (deg)	7.978 to 135.01	626 to 151.018
obsd reflns	23603	22105
R_1[a][I>2σ (I)]	0.0920,	0.0540
wR_2[b] (all data)	0.2773	0.1398

[a] $R_1 = \sum | |Fo| - |Fc| | / \sum |Fo|$. [b] $wR_2 = \{\sum [w (Fo^2 – Fc^2)^2] / \sum [w(Fo^2)^2]\}^{1/2}$.

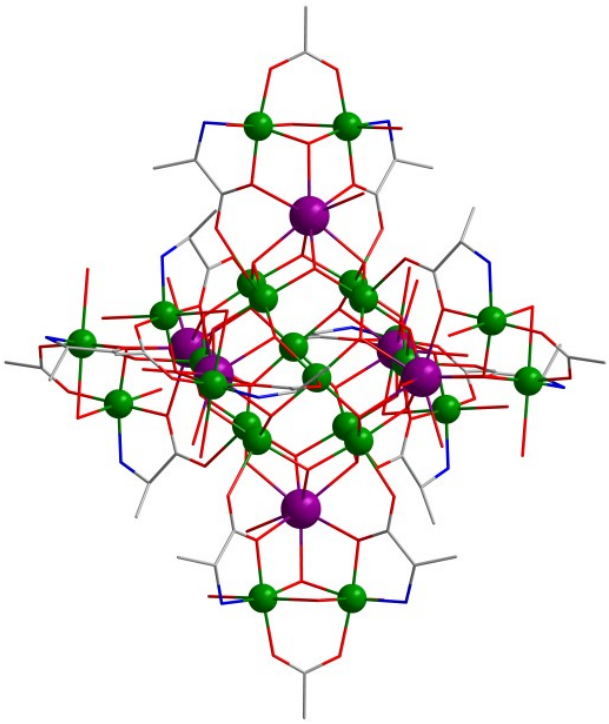

Fig. S1 The core of the **Gd_6Cu_{24}-AC**. Gd: purple, Cu: green, O: red, C: grey, N: blue. All H atoms were omitted.

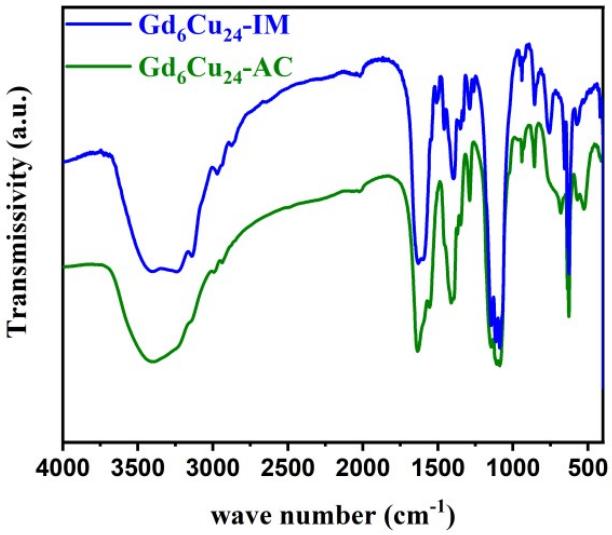

Fig. S2 FT-IR spectra in 500-4000 cm^{-1} for **Gd_6Cu_{24}-IM**, **Gd_6Cu_{24}-AC**.

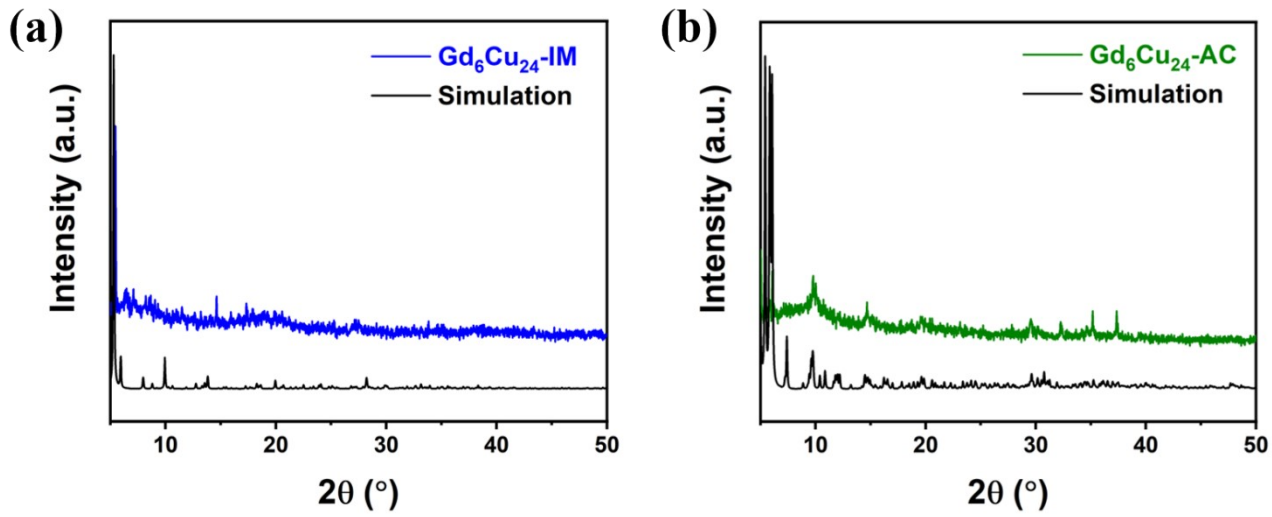

Fig. S3 XRD spectra of **Gd_6Cu_{24}-IM**, **Gd_6Cu_{24}-AC**.

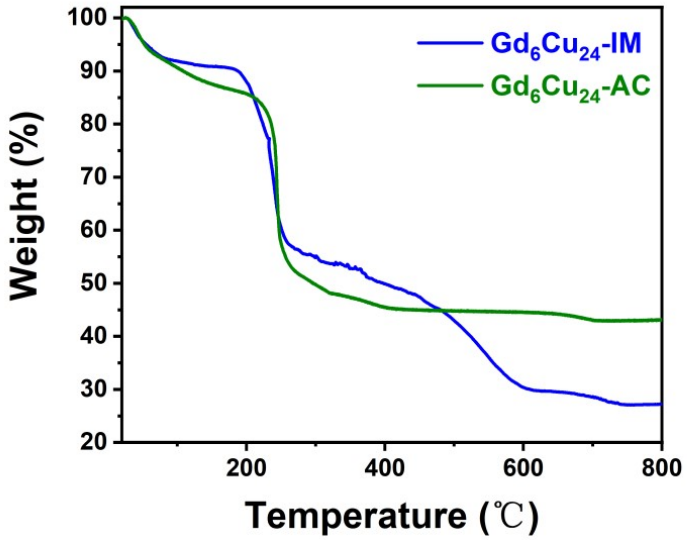

Fig. S4 The TGA measurement of **Gd_6Cu_{24}-IM**, **Gd_6Cu_{24}-AC** under atmosphere.

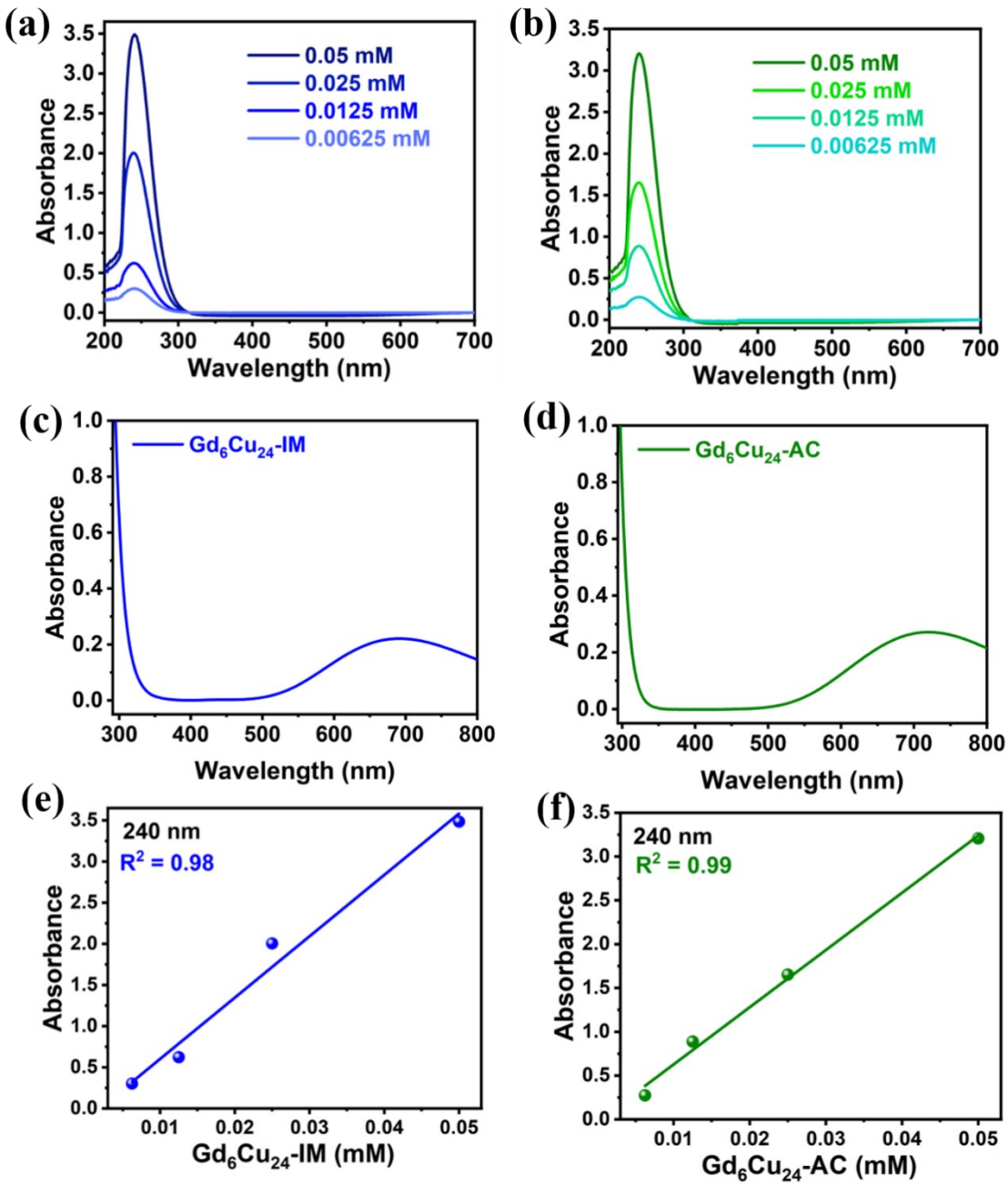

Fig. S5 (a-b) UV-Vis spectra of 0.05 mM, 0.025 mM, 0.125 mM and 0.00625 mM **Gd_6Cu_{24}-IM** (a) and **Gd_6Cu_{24}-AC** (b) in 0.5 M NaAc/HAc buffer solution (pH = 6). (c-d) UV-Vis spectra of 0.25 mM **Gd_6Cu_{24}-IM** (c) and **Gd_6Cu_{24}-AC** (d) in 0.5 M NaAc/HAc buffer solution (pH = 6). e,f) The concentration dependence curves of absorbance of **Gd_6Cu_{24}-IM** (e) and **Gd_6Cu_{24}-AC** (f) at 240 nm. The linear correlation of absorbance to concentration indicates the stability of **Gd_6Cu_{24}-IM** and **Gd_6Cu_{24}-AC** clusters in aqueous solution.

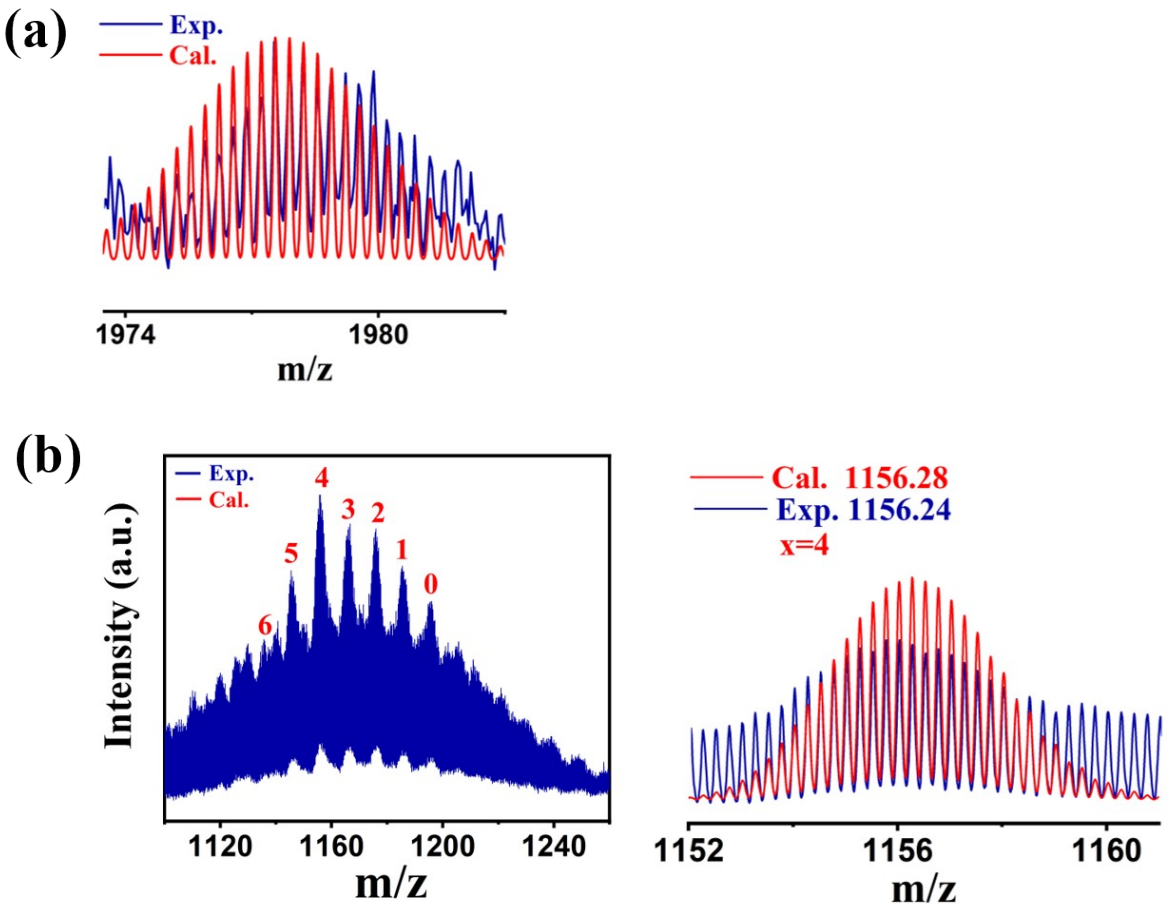

Fig. S6 The high-resolution electrospray ionization mass spectrometry (HRESI-MS) spectra are obtained in aqueous solution of **Gd_6Cu_{24}-IM** (a) and **Gd_6Cu_{24}-AC** (b). For **Gd_6Cu_{24}-IM** (a), the peak at 1978.73 can be attributed to $[Gd_6Cu_{24}(IM)_{12}(L\text{-}Al)_{12}(\mu_3\text{-}OH)_{28}(\mu_3\text{-}O)_8(CO_3)_1(H_2O)_{24}(ClO_4)_5]^{3+}$ (cal. 1978.79). For **Gd_6Cu_{24}-AC** (b), these peaks are observed and can be attributed to $[Gd_6Cu_{24}(Ac)_x(L\text{-}Al)_{10}(\mu_3\text{-}OH)_{28}(\mu_3\text{-}O)_8(H_2O)_2(ClO_4)_{8-x}]^{4+}$ (X=0–6), experimental peaks (blue) versus calculated isotope patterns (red).

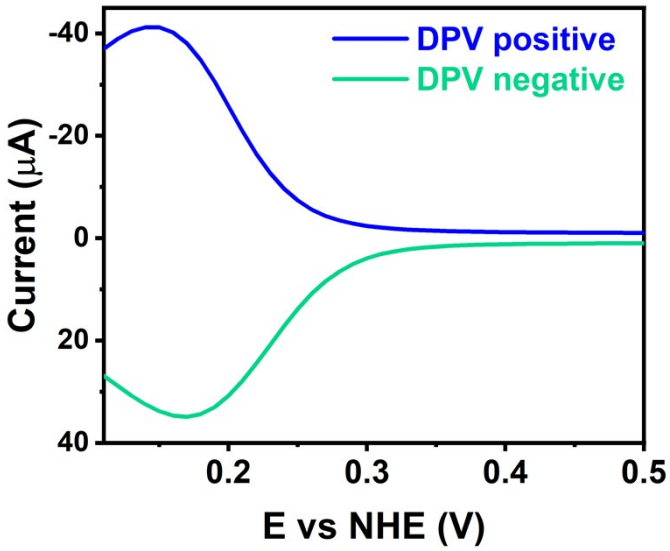

Fig. S7 DPV of 0.25 mM **Gd_6Cu_{24}-IM** in 0.5 M NaAc/HAc (pH = 6) buffer solution using GC electrode at 0-0.5 V.

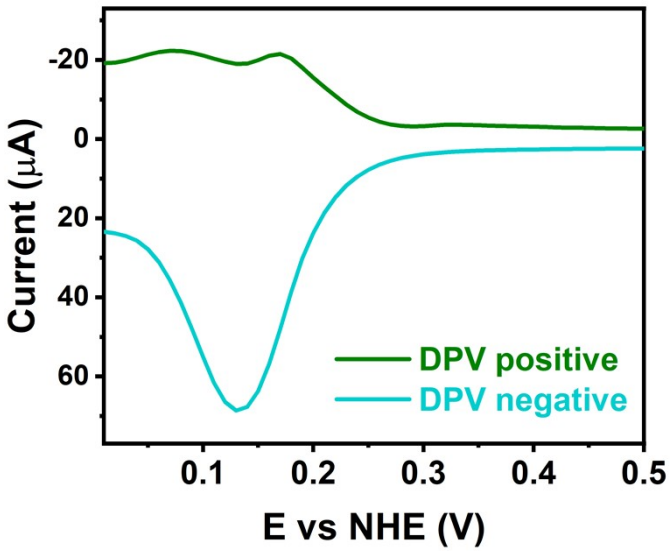

Fig. S8 DPV of 0.25 mM **Gd_6Cu_{24}-AC** in 0.5 M NaAc/HAc (pH = 6) buffer solution using GC electrode at 0-0.5 V.

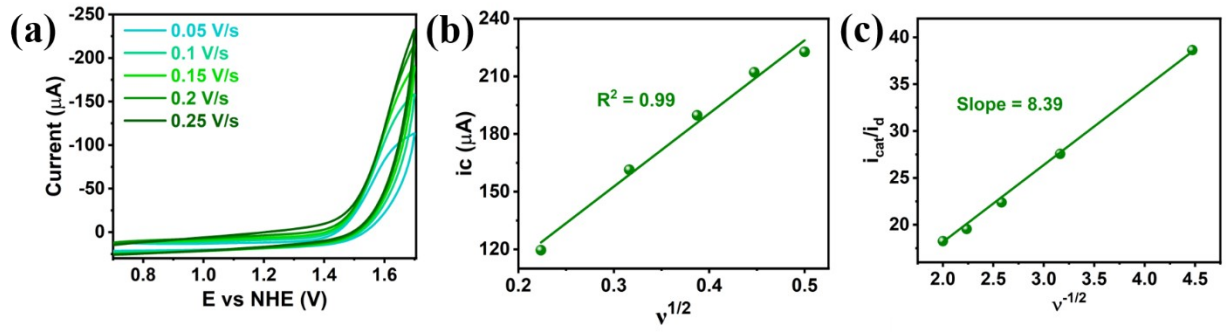

Fig. S9 (a) CV of 0.25 mM **Gd_6Cu_{24}-AC** in 0.5 M NaAc/HAc (pH = 6) buffer solution using GC electrode with different scan rates (0.05-0.25 V s^{-1}) at 0.7-1.7 V. (b) Plots of i_{cat} (μA) vs. $\nu^{1/2}$ ($V^{1/2}$ $s^{-1/2}$) for **Gd_6Cu_{24}-AC**. (c) Plot of the ratio of the catalytic current at 1.70 V, i_{cat}, to the oxidative peak current for the $Gd_6Cu_{24}^{II}/Gd_6Cu_{22}^{II}Cu_2^{III}$ wave, id, vs. $\nu^{-1/2}$.

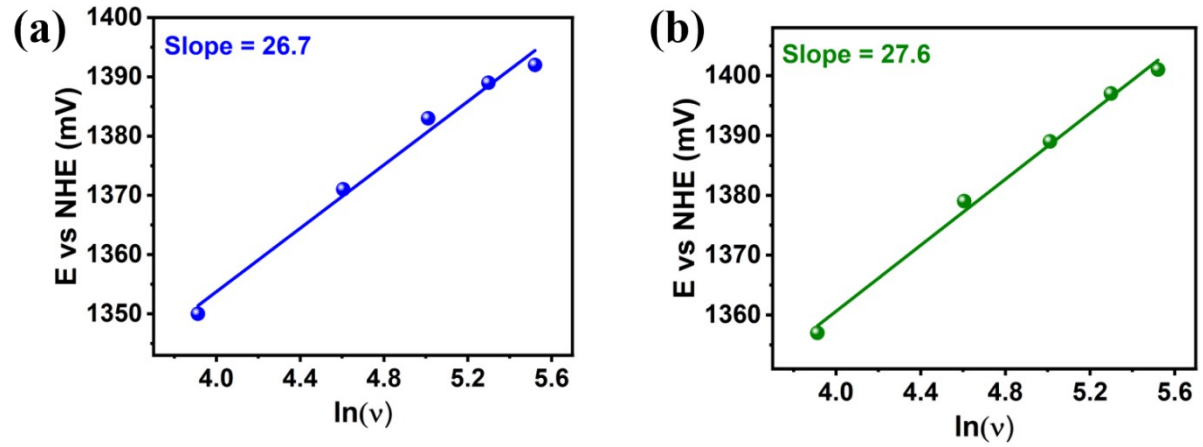

Fig. S10 $E_{p/2}$ of **Gd_6Cu_{24}-IM** (a) and **Gd_6Cu_{24}-AC** (b) as a function of ln (ν). The data were collected from CVs of **Gd_6Cu_{24}-IM** and **Gd_6Cu_{24}-AC** for the $Gd_6Cu_{24}^{II}/Gd_6Cu_{22}^{II}Cu_2^{III}$ couple, respectively (Figure 2b and Figure S8). The fitting results were shown with the straight line.

Determination of the number of electron transfer: The experimental plots were fitted to the straight lines with slope of 26.7 and 27.6 for the anodic shoulder peak $E_{p/2}$ of **Gd_6Cu_{24}-IM** and **Gd_6Cu_{24}-AC**, respectively (Figure S9). $E_{p/2}$ ($i = i_{p/2}$)was utilzed in Laviron equation：

$$E_{p/2} = E_p - 47.7/\alpha n = ℂ + [RT/(1-\alpha)nF] \ln(\nu)$$

α is the transfer coefficient (= 0.5), ℂ is on behalf of the constant. n can then be calculated to be 2.

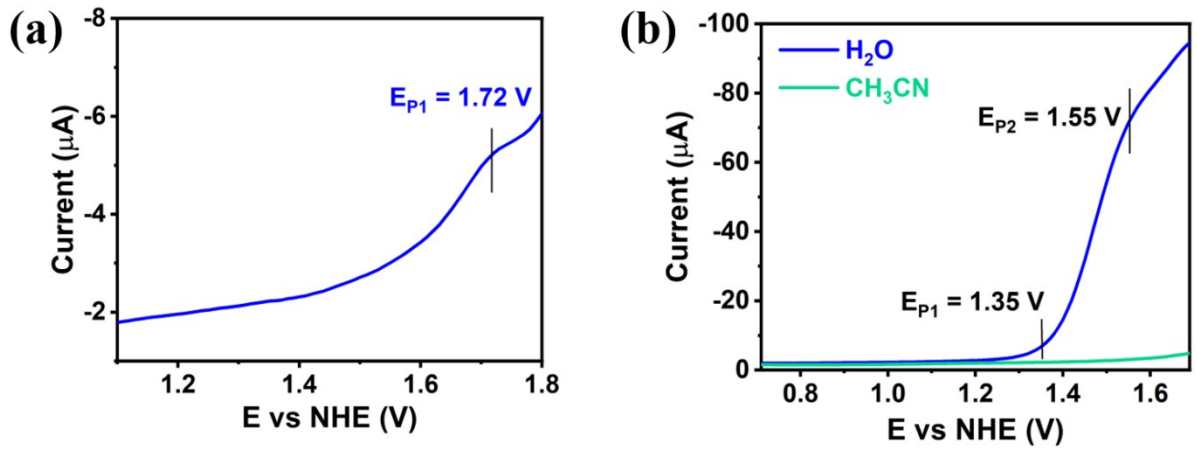

Fig. S11 (a) DPV of 0.25 mM **Gd_6Cu_{24}-IM** in CH_3CN with 0.1 M Et_4NClO_4. (b) DPV of 0.25 mM **Gd_6Cu_{24}-IM** in 0.5 M NaAc/HAc (pH = 6) buffer solution (black line) and CH_3CN with 0.1 M Et_4NClO_4 (red line).

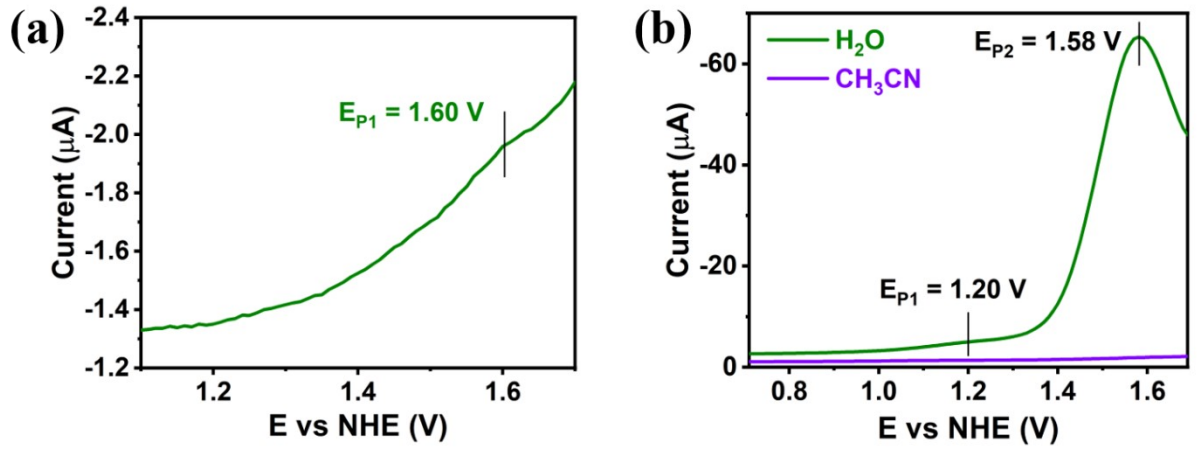

Fig. S12 (a) DPV of 0.25 mM **Gd_6Cu_{24}-AC** in CH_3CN with 0.1 M Et_4NClO_4. (b) DPV of 0.25 mM **Gd_6Cu_{24}-AC** in 0.5 M NaAc/HAc (pH = 6) buffer solution (black line) and CH_3CN with 0.1 M Et_4NClO_4 (red line).

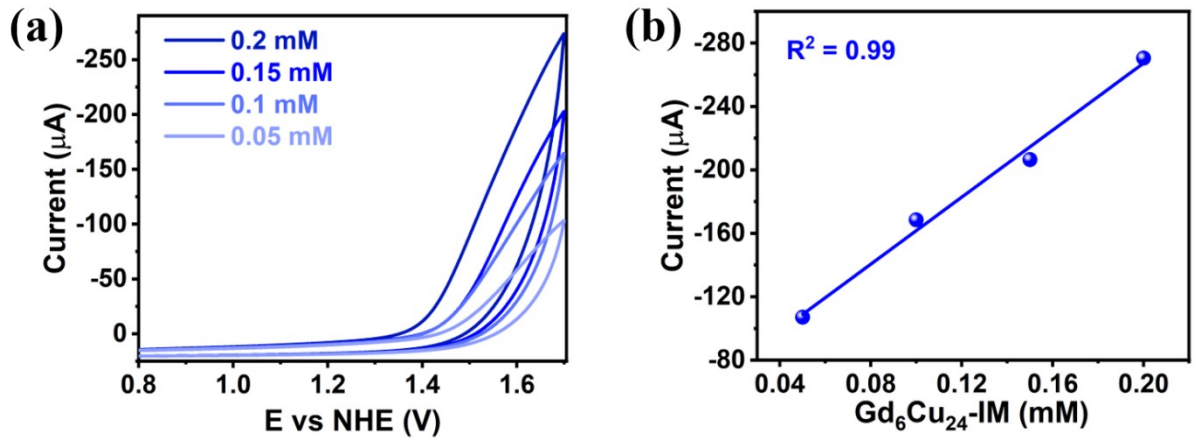

Fig. S13 (a) CV for different concentrations of **Gd_6Cu_{24}-IM** in 0.5 M NaAc/HAc (pH = 6) buffer solution. (b) Plot of the catalytic current icat at 1.70 V versus concentrations of **Gd_6Cu_{24}-IM**.

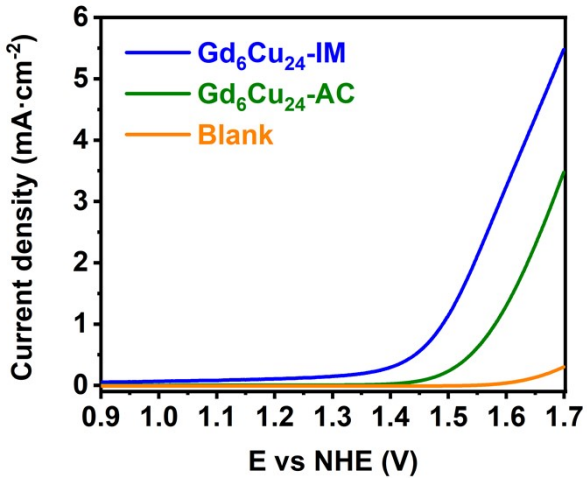

Fig. S14 LSV of 0.25 mM **Gd_6Cu_{24}-IM** and **Gd_6Cu_{24}-AC** in 0.5 M pH=6 NaAc/HAc buffer solution using ITO electrode, scan rate = 100 mV/s.

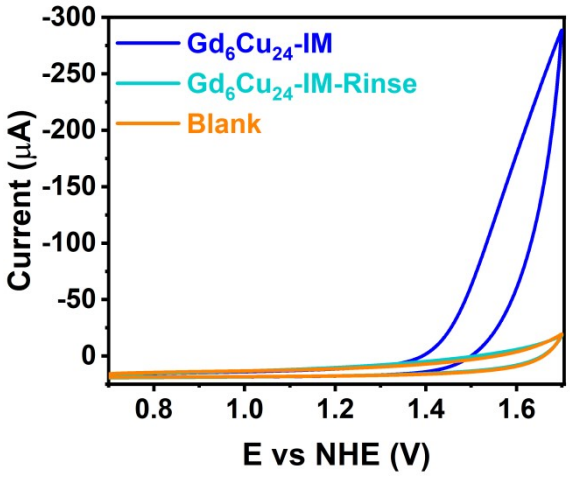

Fig. S15 CV of 0.25 mM **Gd_6Cu_{24}-IM** in 0.5 M NaAc/HAc (pH = 6) buffer solution (black) and a subsequent CV using the same electrode after rinsing and transfer to fresh in 0.5 M NaAc/HAc (pH = 6) buffer solution without adding **Gd_6Cu_{24}-IM** (red). For comparison, CV of 0.5 M NaAc/HAc (pH = 6) buffer solution without **Gd_6Cu_{24}-IM** is shown in green.

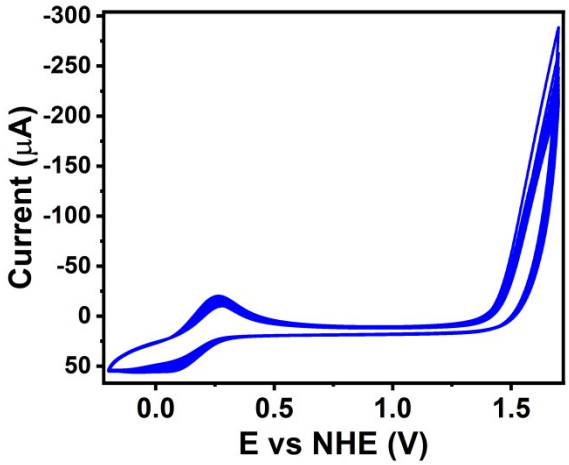

Fig. S16 Continuous CV scans of **Gd_6Cu_{24}-IM** over 50 cycles in 0.5 M NaAc/HAc buffer solution (pH =6).

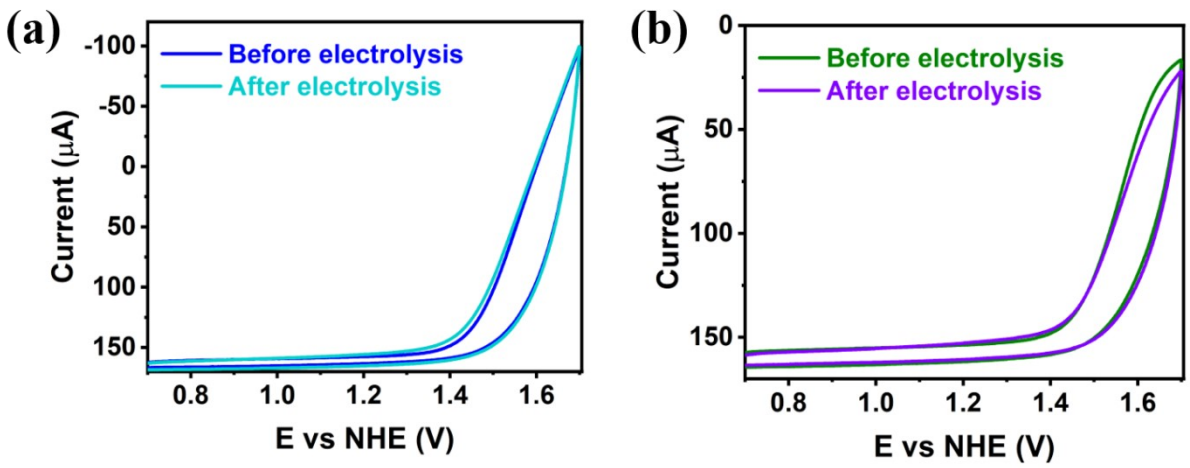

Fig. S17 CV scans before and after 3 hours controlled potential electrolysis of 0.25 mM **Gd_6Cu_{24}-IM** (a) and **Gd_6Cu_{24}-AC** (b) in 0.5 M pH=6 NaAc/HAc buffer solution (pH = 6).

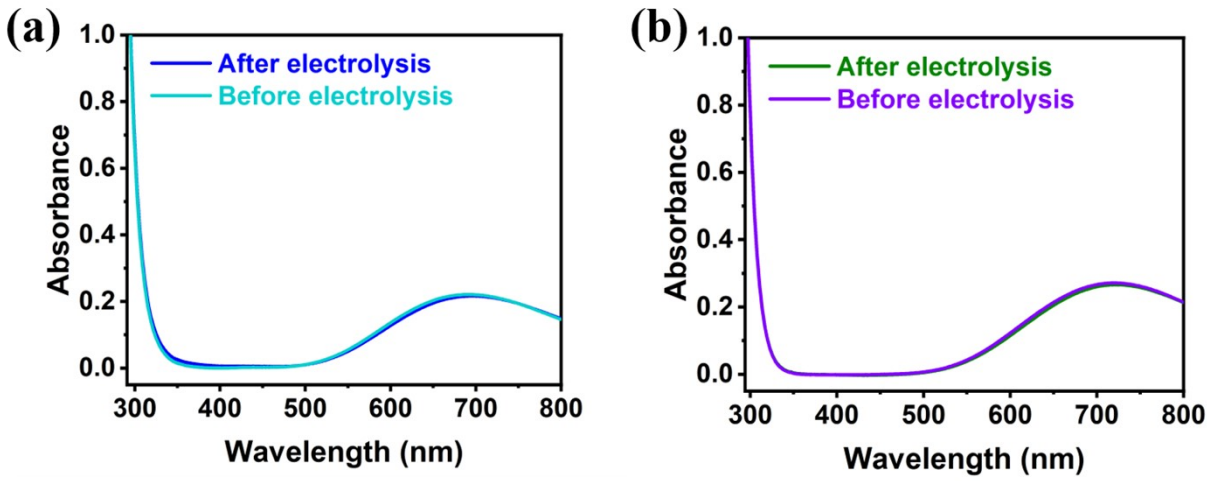

Fig. S18 The UV-Vis spectra of 0.25 mM **Gd_6Cu_{24}-IM** (a) and **Gd_6Cu_{24}-AC** (b) in 0.5 M NaAc/HAc buffer solution (pH = 6) before and after 3 hours controlled potential electrolysis.

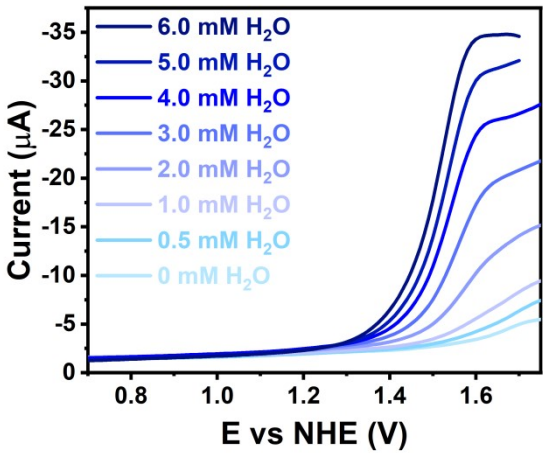

Fig. S19 DPVs of 0.25 mM **Gd_6Cu_{24}-IM** in CH_3CN with 0.1 M Et_4NClO_4 before and after addition of various amounts of H_2O.

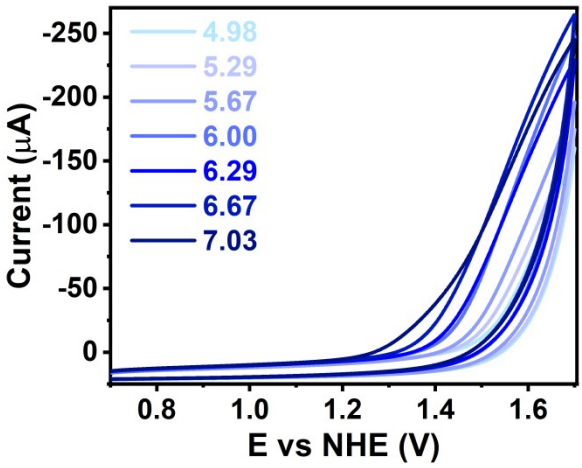

Fig. S20 CVs for 0.25 mM **Gd_6Cu_{24}-IM** in 0.5 M NaAc/HAc (pH 4.98-7.03) buffer solution.

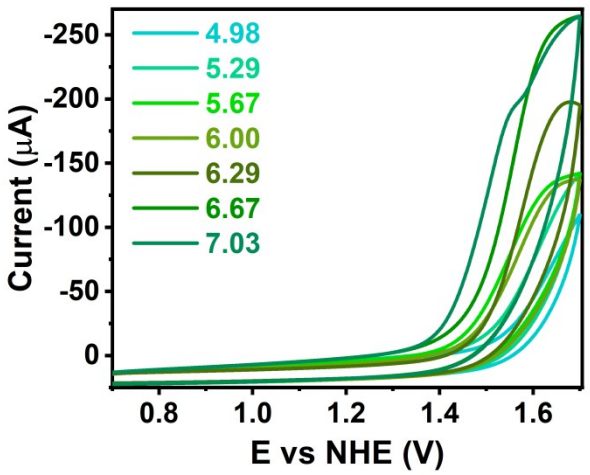

Fig. S21 CVs for 0.25 mM **Gd_6Cu_{24}-AC** in 0.5 M NaAc/HAc (pH 4.98-7.03) buffer solution.

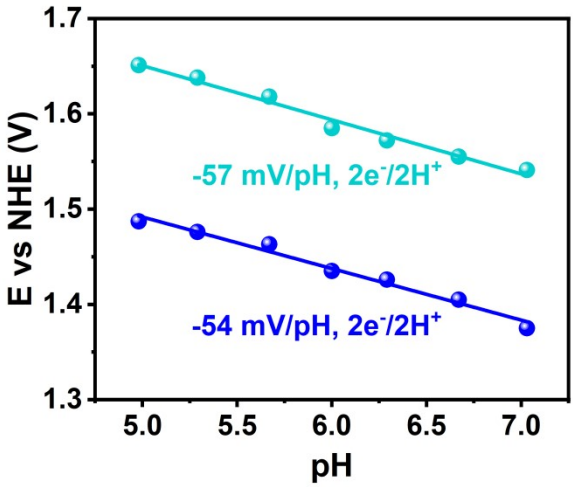

Fig. S22 Pourbaix diagram of 0.25 mM **Gd_6Cu_{24}-IM** in 0.5 M NaAc/HAc (pH 4.98-7.03) buffer solution. Ep values are cited rather than $E_{1/2}$ due to chemical irreversibility.

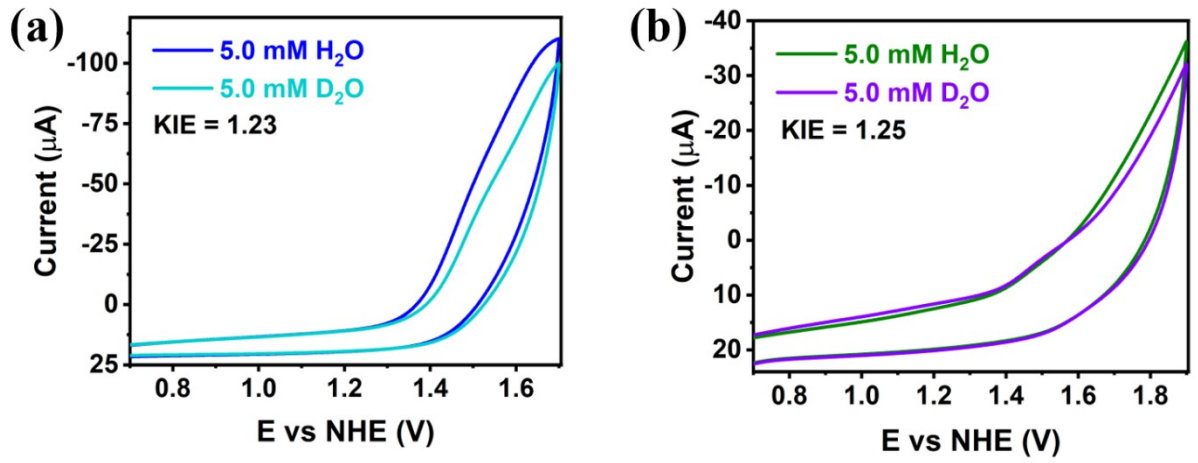

Fig. S23 CV of 0.25 mM **Gd_6Cu_{24}-IM** (a) and **Gd_6Cu_{24}-AC** (b) in CH_3CN (0.1 M Et_4NClO_4) with 5.0 mM H_2O (black line) and D_2O (red line).

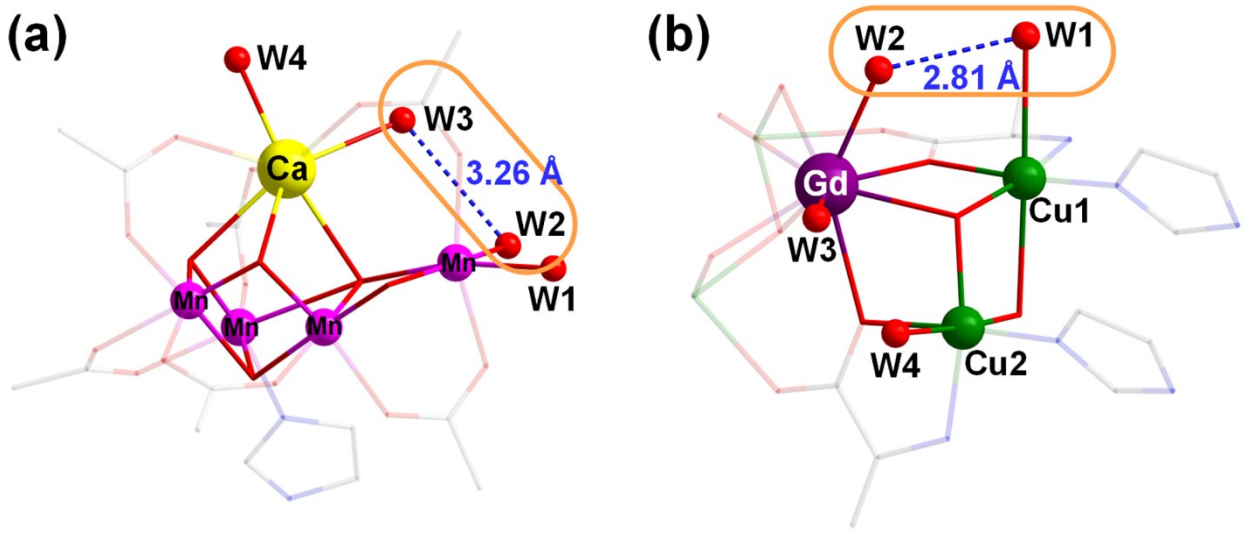

Fig. S24 (a) The structure of the OEC, two molecules of water (W2 and W3) were suggested to provide the oxygen atoms to form the O-O bond. (b) The asymmetric unit [$GdCu_4$] of **Gd_6Cu_{24}-IM**, two molecules of water (W1 and W2) were suggested to provide the oxygen atoms to form the O-O bond.

Table S2 The summary of the catalysts for electrocatalytic water oxidation.

Catalysts	pH	TOF (s^{-1})	Overpotential (mV)	Ref.
$[Fe^{II}_4Fe^{III}(\mu_3\text{-}O)(\mu\text{-}L)_6]^{3+}$	-	1900	>500	[3]
$[(\alpha\text{-}SbW_9O_{33})_2Cu_3(H_2O)_3]^{12-}$	7.1	0.7	-	[4]
$[Cu_4(pdmH)_4(OAc)_2](NO_3)_2\cdot 3H_2O$	11.78	0.26	400	[5]
$[Cu_4(bpy)_4(\mu_2\text{-}OH)_2(\mu_3\text{-}OH)_2(H_2O)_2]^{2+}$	7	-	730	[6]
$[Cu_2(TPMAN)(\mu\text{-}OH)(H_2O)]^{3+}$	7	0.78	780	[7]
$[Cu(Me_2oxpn)Cu(OH)_2]$	10.4	2.14	636	[8]
$Mn_{12}DH$	6	0.035	334	[9]
$Mn_{12}TH$	6	22	74	[10]
$[(L_{Gly}\text{-}Cu)_4]$	12	267	620	[11]
$[(L_{Glu}\text{-}Cu)_4]$	12	105	760	[11]
$[Cu_4(H_2L)_4](ClO_4)_4$	12.5	0.8	500	[12]
$[Co_9(H_2O)_6(OH)_3(HPO_4)_2(PW_9O_{34})_3]^{16-}$	7	-	353	[13]
$[Cu_2(BPMAN)(\mu\text{-}OH)]^{3+}$	7	-	800	[14]
$[Cu_3(pda)_3(tBuPO_3)]\cdot 2(Et_3NH)$	7	0.82	800	[15]
$[Cu_3(pda)_3(PhPO_3)]\cdot 2(Et_3NH)$	7	0.58	800	[15]
$[Mn_4(H_2O)_2(PW_9O_{34})_2]^{10-}$	7	-	600	[16]
Cu_3L	11	-	620	[17]
$Eu_{36}Co_{12}$	5.8	1.5	700	[18]
$[(DAM)Cu_3(\mu_3\text{-}O)](Cl)_4$	11.4	122.6	800	[19]
$[(app^{2-})Cu^{II}_3(\mu\text{-}OH)](CF_3SO_3)_3$	8.4	20000	910	[20]
Gd_6Cu_{24}-IM	6	319	598	**This work**
Gd_6Cu_{24}-AC	6	169	689	**This work**

References

1 G. M. Sheldrick, SADABS 2.05; University of Göttingen: Göttingen, Germany.

2 Bruker. SHELXTL, version 5.10; Bruker AXS Inc.: Madison, WI, 1997.

3 M. Okamura, M. Kondo, R. Kuga, Y. Kurashige, T. Yanai, S. Hayami, V. K. K. Praneeth, M. Yoshida, S. Kawata, M. Shigeyuki. *Nature*, 2016, **530**, 465-468.

4 L. Yu, J. Lin, M. Zheng, M. Chen, Y. Ding. *Chem. Commun.*, 2018, **54**, 354-357.

5 W. S. Gao, J. M. Wang, N. N. Shi, C. N. Chen, Y. Fan, M. Wang. *New J. Chem.*, 2019, **43**, 4640-4647.

6)T. T. Lia, Y. Q. Zheng. *Dalton Trans.*, 2016, **45**, 12685-12690.

7 Q. Q. Hu, X. J. Su, M. T. Zhang. *Inorg. Chem.*, 2018, **57**, 10481-10484.

8 L. L. Zhou, T. Fang, J. P. Cao, Z. H. Zhu, X. T. Su, S. Z. Zhan. *J. Power Sources*, 2015, **273**, 298-304.

9 G. Maayan, N. Gluz, G. Christou. *Nat. Catal.*, 2018, **1**, 48-54.

(10) T, Ghosh, G, Maayan. *Angew. Chem. Int Ed.*, 2019, **58**, 2785-2790.

11 X. Jiang, J. Li, B. Yang, X. Z. Wei, B. W. Dong, Y. Kao, M. Y. Huang, C. H. Tung, L. Z. Wu. *Angew. Chem. Int. Ed.*, 2018, **57**, 7850-7854.

12 V. K. K. Praneeth, M. Kondo, P. Woi, M. Okamura, S. Masaoka. *ChemPlusChem*, 2016, **81**, 1123-1128.

13 S. Goberna-Ferrón, L. Vigara, J. Soriano-López, J. R. Galán-Mascarós. *Inorg. Chem.*, 2012, **51**, 11707-11715.

14 X. J. Su, M. Gao, L. Jiao, R. Z. Liao, P. E. M. Siegbahn, J. P. Cheng, M. T. Zhang. *Angew. Chem. Int. Ed.*, 2015, **54**, 4909-4914.

15 J. M. Wang, Y. R. Liu, X. Y. Mao, N. N. Shi, X. Zhang, H. S. Wang, Y. H. Fan, M. Wang. *Chem. Asian J.*, 2019, **14**, 2685-2693.

16 S. Goberna-Ferrón, J. Soriano-López, J. R. Galán-Mascarós. *Inorganics*, 2015, **3**, 332-340.

17 Ł. Szyrwiel, D. Lukács, T. Ishikawa, J. Brasun, Ł. Szczukowski, Z. Szewczuk, B. Setner, J. S. Pap. *Catal. Commun.*, 2019, **122**, 5-9.

18 R. Chen, C. L. Chen, M. H. Du, X. Wang, C. Wang, L. S. Long, X. J. Kong, L. S. Zheng. *Chem. Commun.,* 2021, **57**, 3611-3614.

19 A. M. Geer, C. Musgrave, C. Webber, R. J. Nielsen, B. A. McKeown, C. Liu, P. P. M. Schleker, P. Jakes, X. F. Jia, D. A. Dickie, J. Granwehr, S. Zhang, C. W. Machan, W. A. Goddard, T. B. Gunnoe. *ACS. Catal.*, 2021, **11**, 7223-7240.

20 Q. F. Chen, Z. Y. Cheng, R. Z. Liao, M. T. Zhang. Bioinspired Trinuclear Copper Catalyst for Water Oxidation with a Turnover Frequency up to 20000 s^{-1}. *J. Am. Chem. Soc.,* 2021, **143**, 19761-19768.